Discovering a novel D-xylonate-responsive promoter: the P_{yjhI}-driven genetic switch towards better 1,2,4-butanetriol production

Angelo B. Bañares[1] · Kris Niño G. Valdehuesa[1] · Kristine Rose M. Ramos[1] · Grace M. Nisola[1] · Won-Keun Lee[2] ·
Wook-Jin Chung[1] (ORCID)

Abstract

The capability of *Escherichia coli* to catabolize D-xylonate is a crucial component for building and optimizing the Dahms pathway. It relies on the inherent dehydratase and keto-acid aldolase activities of *E. coli*. Although the biochemical characteristics of these enzymes are known, their inherent expression regulation remains unclear. This knowledge is vital for the optimization of D-xylonate assimilation, especially in addressing the problem of D-xylonate accumulation, which hampers both cell growth and target product formation. In this report, molecular biology techniques and synthetic biology tools were combined to build a simple genetic switch controller for D-xylonate. First, quantitative and relative expression analysis of the gene clusters involved in D-xylonate catabolism were performed, revealing two D-xylonate-inducible operons, *yagEF* and *yjhIHG*. The 5′-flanking DNA sequence of these operons were then subjected to reporter gene assays which showed P_{yjhI} to have low background activity and wide response range to D-xylonate. A P_{yjhI}-driven synthetic genetic switch was then constructed containing feedback control to autoregulate D-xylonate accumulation and to activate the expression of the genes for 1,2,4-butanetriol (BTO) production. The genetic switch effectively reduced D-xylonate accumulation, which led to 31% BTO molar yield, the highest for direct microbial fermentation systems thus far. This genetic switch can be further modified and employed in the production of other compounds from D-xylose through the xylose oxidative pathway.

Keywords D-Xylonate · Dahms pathway · yjhI promoter · Genetic switch · 1,2,4-Butanetriol

Introduction

The Dahms and Weimberg pathways have been gaining attention for D-xylose metabolism during the recent years. Unlike the traditional D-xylose isomerase or reductase pathways, the Dahms and Weimberg pathways begin with the oxidation of D-xylose to D-xylonate. Hence, both pathways are collectively called the D-xylose oxidative pathways (XOP) (Valdehuesa et al. 2018). D-Xylonate then undergoes two to four more reactions to form pyruvate or 2-ketoglutarate (Dahms 1974; Weimberg 1961). The XOP has been found in strains belonging to the Archaea and Bacteria domains (Brouns et al. 2006; Stephens et al. 2007) and was engineered in several industrial strains (Cabulong et al. 2018a; Radek et al. 2014; Salusjärvi et al. 2017). Interestingly, recruiting the Dahms pathway in *Escherichia coli* only requires the expression of a non-native xylose dehydrogenase (EC 1.1.1.179) to catalyze the oxidation of D-xylose to form D-xylonate, which *E. coli* apparently has the capability to assimilate (Liu et al. 2013).

The inherent D-xylonate assimilative route in *E. coli* involves two steps: D-xylonate dehydration and a keto-acid aldol cleavage reaction (Fig. 1a). These enzymes appear to be unique to the K-12 strain and its derivatives, with the respective genes clustered in *yag* or *yjh* regions of the genome (Fig. 1b). From this pre-existing set of genes, the full XOP

Angelo B. Bañares and Kris Niño G. Valdehuesa contributed equally to this work.

Electronic supplementary material The online version of this article (https://doi.org/10.1007/s00253-019-10073-0) contains supplementary material, which is available to authorized users.

✉ Won-Keun Lee
   wklee@mju.ac.kr

✉ Wook-Jin Chung
   wjc0828@gmail.com

[1] Department of Energy Science and Technology (DEST), Energy and Environment Fusion Technology Center (E2FTC), Myongji University, Myongji-ro 116, Cheoin-gu, Yongin 17058, Gyeonggi-do, Republic of Korea

[2] Division of Bioscience and Bioinformatics, Myongji University, Myongji-ro 116, Cheoin-gu, Yongin 17058, Gyeonggi-do, Republic of Korea

Fig. 1 **a** Metabolic route for D-xylonate assimilation in *E. coli* K-12 strains. **b** *yag* and *yjh* gene clusters in *E. coli* W3110 genome. The gene products are indicated above the open-reading frame; numbers indicate location of the operon in the genome map; TF, transcription factor
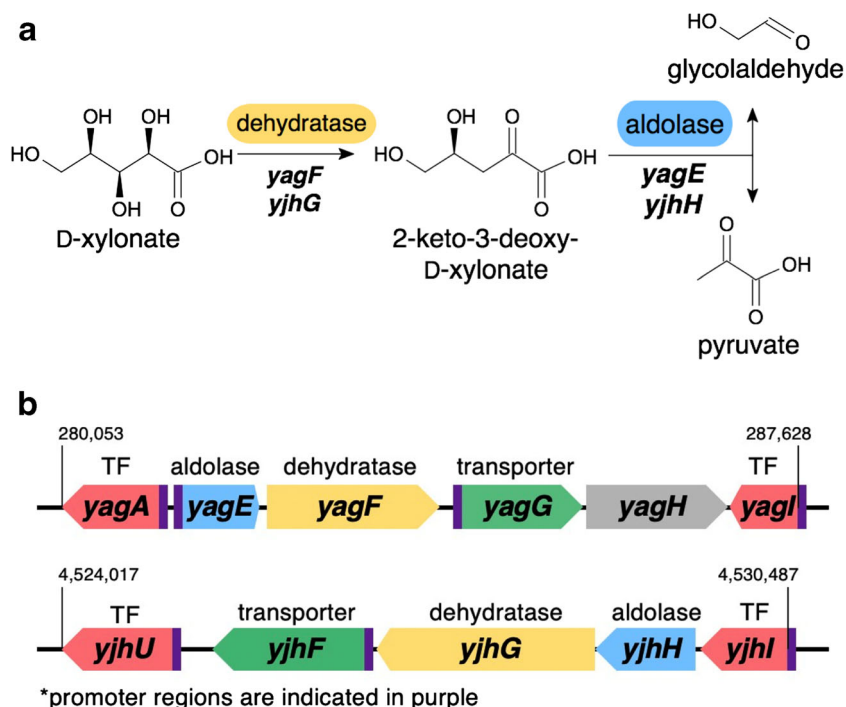
was built in *E. coli*, thus, allowing the conversion of D-xylose to ethylene glycol, glycolic acid, 1,4-butanediol, and 1,2,4-butanetriol (BTO) (Cabulong et al. 2018a; Liu et al. 2013; Liu and Lu 2015; Valdehuesa et al. 2014). Further developments in *E. coli* strains with an optimized XOP were reported by employing traditional metabolic engineering strategies. For example, ethylene glycol yield was improved by modulating the expression of xylose dehydrogenase and overexpressing the best performing aldehyde reductase (EC 1.1.1.2) (Cabulong et al. 2017). Redox homeostasis was restored by overexpression of a transhydrogenase (EC 7.1.1.1), which improved cell growth and glycolic acid yield (Cabulong et al. 2018b). Lastly, BTO production was enhanced by the knockout of competing reactions (Zhang et al. 2016).

Despite the success in engineering the XOP in *E. coli*, a persistent problem exists—the accumulation of D-xylonate. The buildup of D-xylonate in the medium elicits a cascade of stress responses in the host strain. For instance, it reduces the pH of the media which makes the conditions unsuitable for optimum growth and enzymatic functions (Liu et al. 2012; Valdehuesa et al. 2014). As mentioned above, the *E. coli* host strain is equipped with the necessary enzymes to assimilate D-xylonate; hence, its accumulation is very uncharacteristic. There is no doubt that these enzymes catalyze the right reactions for the pathway to work because their activities have been confirmed through enzyme assays (Jiang et al. 2015; Liu et al. 2013; Valdehuesa et al. 2018). However, the knowledge about the regulation of these enzymes is non-existent. Uncovering the regulatory mechanisms of the pathway would

be essential in understanding why D-xylonate accumulates persistently in *E. coli* strains that were engineered to assimilate D-xylose through the XOP. It would also provide insights into how to manipulate the strain to minimize D-xylonate accumulation.

In the present study, investigations on the inherent D-xylonate assimilative pathway in *E. coli* were performed. Biomolecular experiments involving relative expression analysis, reporter gene assays, and deletion mapping experiments identified a novel D-xylonate-responsive promoter. This promoter was further tested and used in building a genetic switch for the dynamic control of D-xylonate accumulation during BTO production in *E. coli*.

Materials and method

DNA manipulations

All recombinant plasmids and strains are listed in Table 1. Standard techniques were used in all genetic manipulation experiments (Green and Sambrook 2012) while Gibson Assembly was used for cloning of recombinant DNA (Gibson et al. 2009). All PCR reactions were carried out using Phusion high-fidelity DNA polymerase. Plasmid transformation was performed using the one-step TSS (transformation and storage solution) protocol (Chung et al. 1989). The *sf*GFP was cloned from *sf*GFP-pBAD, which was generously provided by Michael Davidson and Geoffrey Waldo (Addgene

Table 1 Plasmids and strains names used in this study

Names	Relevant characteristics	Source
Plasmids		
pET28a	pBR322 ori, P_{T7}, Kan^R	Invitrogen
pRSET-A	pUC ori, P_{T7}, Amp^R	Invitrogen
pX	pACM4 with xdh from $Caulobacter\ crescentus$	Cabulong et al. 2018a
pXG	pX with $yjhG$ from $E.\ coli$	Cabulong et al. 2018a
pACM4	pACYC-Duet derivative; with ePathBrick feature; P_{T7}; Cm^r	Xu et al. 2012
pETM6	Vector with ePathBrick feature; P_{T7}; Amp^r	Xu et al. 2012
sfGFP-pBAD	P_{pBAD}-$sfGFP$ (Addgene #54519)	*
pETmCherryLIC	P_{T7}-mCherry, (Addgene #29769)	**
pTRM	pTrcHis2A derivative; expression vector of $mdlC$	Valdehuesa et al. 2014
pTRA1	pTrcHis2A derivative; expression vector of $yqhD$	Valdehuesa et al. 2015
pET28-T7-mCherry	pET28a derivative; $P_{T7\text{-}lacO}$-mCherry	This work
pET28-PyagE-mCherry	pET28a derivative; P_{yagE}-mCherry	This work
pET28-PyjhI-mCherry	pET28a derivative; P_{yjhI}-mCherry	This work
pET28-PyjhI-Sf	pET28a derivative; P_{yjhI}-sfGFP	This work
pR-XAS	pRSET-A derivative; $P_{T7\text{-}lacO}$-mCherry, P_{yjhI}-$lacI$, P_{yjhI}-sfGFP	This work
pR-xdh	pRSET-A derivative; $P_{T7\text{-}lacO}$-xdh	This work
pR-XSEN	pR-xdh derivative; $P_{T7\text{-}lacO}$-xdh, P_{yjhI}-$lacI$	This work
pR-CBT	pR-xdh derivative; $P_{T7\text{-}lacO}$-xdh, P_{yjhI}-$mdlC$-$yqhD$	This work
pR-XSBT	pR-XSEN derivative; $P_{T7\text{-}lacO}$-xdh, P_{yjhI}-$lacI$, P_{yjhI}-$mdlC$-$yqhD$	This work
pR-yqhD	pRSET-A derivative; P_{T7}-$yqhD$	This work
pM-mdlC	pETM6 derivative; $P_{T7\text{-}lacO}$ -$mdlC$	This work
pR-XGD	pRSET-A derivative; P_{T7}-xdh-$yjhG$-$mdlC$	This work
pR-XGCD	pRSET-A derivative; P_{T7}-xdh-$yjhG$-$mdlC$-$yqhD$	This work
Strains		
MG1655 (DE3)	$E.\ coli$ MG1655 (DE3)	ATCC 47076
W3110 (DE3)	$E.coli$ W3110 (DE3) F$^-$ mcrA mcrB IN (rrnD$^-$ rrnE) 1λ$^-$ (DE3)	ATCC 27325
WXHE	W3110 (DE3) $\Delta xylAB$ $\Delta yjhH$ $\Delta yagE$	Valdehuesa et al. 2014
MGMC0	MG1655 (DE3) pET28a	This work
MGMC1	MG1655 (DE3) pET28-T7-mCherry	This work
MGMC2	MG1655 (DE3) pET28-PyagE-mCherry	This work
MGMC3	MG1655 (DE3) pET28-PyjhI-mCherry	This work
WXAS	W3110 (DE3) pR-XAS	This work
WBT+	WXHE pR-XGCD	This work
WBTC	WXHE pR-CBT	This work
WBTXS	WXHE pR-XBST	This work

*sfGFP-pBAD was a gift from Michael Davidson and Geoffrey Waldo (Addgene plasmid # 54519)

**pET mCherry LIC cloning vector was a gift from Scott Gradia (Addgene plasmid # 29769)

plasmid #54519) (Pédelacq et al. 2006). The $mdlc$ and $yqhD$ genes were derived from pTRM (Valdehuesa et al. 2014) and pTRA1 (Valdehuesa et al. 2015), respectively, while $lacI$ was amplified from pACM4 (Table 1). The mCherry was cloned from pETmCherryLIC, which was generously provided by Scott Gradia (Addgene plasmid #29769). The P_{yagE} and P_{yjhI} promoters listed in SI File 1 (SI Table S1)

were PCR amplified using the genomic DNA of $E.\ coli$ W3110 (DE3) as the template. Complete details for cloning the plasmids and strains used for the reporter gene assays, deletion mapping experiments, and the synthetic genetic switches are described in SI File 2. The sequence fidelity of all the constructed plasmids was confirmed by DNA sequencing.

Culture conditions

Plasmid propagation and maintenance were done using *E. coli* DH5α grown on LB broth or agar supplemented with appropriate antibiotics (50 μg mL^{-1} kanamycin or 100 μg mL^{-1} ampicillin). Modified M9 (MM9) medium containing 33.7 mM Na$_2$HPO$_4$, 22.0 mM KH$_2$PO$_4$, 8.55 mM NaCl, 9.35 mM NH$_4$Cl, 1.0 mM MgSO$_4$, 0.5 g L^{-1} yeast extract, and 1.0 g L^{-1} peptone was used throughout the study. A final concentration of 10 mM D-xylose, D-glucose, D-xylonate, or any combination of these substrates were used for real-time PCR (qPCR) experiments. Meanwhile, 20 mM D-xylonate was used for reporter gene assays and genetic switch experiments. Dose-response experiments were performed using D-xylonate concentrations 0 to 100 mM. Whenever necessary, the addition of 0.1 mM isopropyl β-D-1-thiogalactopyranoside (IPTG) was done when OD$_{600}$ reached 0.3 A.U.

Production of BTO was performed in 300-mL shake flasks with 100 mL LB medium supplemented with 10 g L^{-1} of xylose and 100 μg mL^{-1} ampicillin. An overnight culture (100 μL) was inoculated in each flask and incubated with agitation (250 rpm) at 37 °C for 96 to 108 h. At specified time intervals, samples were collected for monitoring of cell growth and metabolite concentrations. The metabolites were quantified using HPLC following the same conditions as described in a previous work (Valdehuesa et al. 2014).

Real-time PCR

Wild-type *E. coli* W3110 strain was used in qPCR experiments. Cells were grown in 50-mL tubes with 5 mL MM9 with the appropriate substrate(s) and incubated at 37 °C for 3 h. Control conditions were designated to cells grown in MM9 media only. Treatment conditions included strains grown with D-xylose, D-glucose, D-xylonate, or any combination of these substrates. Total mRNA of growing cells was purified using the RNeasy Mini Kit (Qiagen, Germany) with modifications in the protocol provided by the manufacturer. Cells from the culture samples were harvested and re-suspended in Tris-EDTA buffer containing lysozyme. The mixture was incubated at room temperature for 5 min prior addition of RLT buffer (included in the kit) and ethanol. The remaining steps for RNA purification were performed according to the protocol provided by the manufacturer (starting with step 3 of the Quick-start protocol RNeasy Mini Kit, Part 1). The quality of isolated RNA was assessed using NanoDrop 1000 spectrophotometer from Thermo Scientific (Waltham, MA, USA) and by agarose gel electrophoresis. RNA was converted to cDNA using the QuantiTect Reverse Transcription kit (Qiagen, Germany) following the manufacturer specifications, which includes a step for removal of genomic DNA. qPCR reactions were performed using the QuantiFast® SYBR® Green PCR Kit (Qiagen, Germany). Each reaction contained appropriate qPCR primers (SI Table S2) with a final concentration of 1 μM. Reference genes *rrsB*, *mdoG*, and *cysG* were used to allow adequate normalization of expression levels of the target genes. The qPCR reactions were performed using Rotor-Gene Q (Qiagen, Germany) with 40 cycles of denaturation at 95 °C, and annealing and extension at 62 °C for 10 s.

Reporter gene assays (fluorescence analysis)

A 1-mL aliquot of overnight culture prepared in LB broth was harvested and washed once with sterile MM9 media. The washed cells were re-suspended in 500 μL MM9 media and inoculated to 25 mL fresh MM9 media in 100-mL shake flasks. The initial OD$_{600}$ values for each culture was around 0.03–0.05 and the flasks were incubated at 37 °C with 250 rpm agitation. Sugar inducers were added when OD$_{600}$ reached 0.4 A.U. and the samples collected at this time was set at 0 h. For the positive control (pET28-T7-mCherry), 0.1 mM IPTG was added in lieu of any inducing sugar. For normalization, sample collection volume was adjusted based on the OD$_{600}$ equivalent to 1 per milliliter. The samples were then centrifuged at 21,206×*g* for 2 min and re-suspended in 1 mL sterile water. Fluorescence was measured using FluoroMate FS-2 (Scinco, Korea) at the following parameters: 587-nm excitation and 610-nm emission for sfGFP; 485-nm excitations and 507-nm emission for mCherry.

Bioinformatics studies

Promoter sequences were analyzed using the online tool BPROM—prediction of bacterial promoters (Solovyev and Salamov 2011; Umarov and Solovyev 2017) and Neural Network Promoter Prediction (NNPP) (Reese 2001). DNA curvature and %GC content were analyzed using bend.it® (Vlahoviček et al. 2003).

Gene accession numbers

The following are the gene accession numbers (GeneID) of the genes mentioned in this work: *yagB* (944944), *yagA* (944937), *yagE* (944925), *yagF* (944928), *yagG* (944947), *yagH* (944949), *yagI* (xynR, 945,016), *yjhI* (949110), *yjhH* (948825), *yjhG* (946829), *yjhF* (949102), *yjhU* (948827), *yqhD* (947493), *xdh* (MF872191), and *mdlC* (882177).

Results

yag and *yjh* genes induced by D-xylonate

Preliminary experiments were performed to confirm the inducibility of the structural and regulatory genes in the *yag* and *yjh* gene clusters in *E. coli* MG1655 towards D-xylonate

as inducer. As mentioned above, these genes were previously shown to be involved in D-xylonate metabolism of *E. coli* (Fig. 1). The predicted transporter-coding genes, *yagG* and *yjhF*, were excluded as they are likely to be constitutively expressed. Results show that the structural genes *yjhG*, *yjhH*, and *yagE* have increased expressions in the presence of D-xylonate when compared to cells grown under control conditions (MM9 media only) (Fig. 2a). Genes predicted as transcription factors (*yagA*, *yagI*, and *yjhU*) have lower expressions in cells exposed to D-xylonate. On the other hand, the structural genes in both gene clusters have increased expressions in D-xylonate-treated cells compared to those incubated with D-xylose (Fig. 2b). The transcript levels of *yagA* and *yjhU* did not have any difference, while *yagI* showed a very low $\log_2$ value (Fig. 2b). Transcript quantification experiments also revealed that *yagE* and *yagF* have significantly higher mRNA counts in D-xylonate-treated cells (SI Fig. S1A). Furthermore, the transcript levels of *yjhG*, *yjhH*, *yjhI*, and *yjhU* were also higher in the presence of D-xylonate (SI Fig. S1B). This indicated that the genes in both clusters (or at least the transcripts that encoded structural genes) are inducible by D-xylonate.

Further quantitative expression analysis revealed no significant differences in the transcript levels in all the genes of interest in cells treated with D-glucose or D-xylose compared to cells grown in control conditions (SI Fig. S1). However, these transcript levels were generally lower when compared to D-xylonate-treated cells. Additionally, the presence of D-glucose combined with D-xylonate had a negative influence on the overall transcript levels when compared to cells treated with only D-xylonate (Fig. 2c). This behavior was also observed when the transcript levels were compared to cells treated with only D-xylose (Fig. 1c). Taken together, these results initially indicate that both gene clusters may be influenced by carbon catabolite repression (CCR), which was forthcoming since the majority of the carbon assimilative pathways in *E. coli* are under the control of CCR (Beisel and Afroz 2016; Görke and Stülke 2008).

As shown in Fig. 1b, *yagE* and *yagF* genes are predicted to belong to a single transcript while *yjhI*, *yjhH*, and *yjhG* genes belong to another. As these genes appear to be induced by the presence of D-xylonate, the 5′-flanking sequences of each operon were suggested to contain D-xylonate-responsive promoters. Accordingly, the 294 bp DNA sequence flanking the 5′-end of *yagE* was designated as P_{yagE} while the 302 bp DNA upstream the 5′-end of *yjhI* was designated as P_{yjhI} (SI Table S5). Reporter gene assays for P_{yagE} and P_{yjhI} were done to test their corresponding promoter activities. Both promoters were individually cloned upstream of the mCherry reporter gene (red fluorescent protein) (SI Fig. S2) and were expressed in *E. coli* MG1655 (DE3). As a control, mCherry was also expressed under the IPTG-inducible T7 promoter. Results
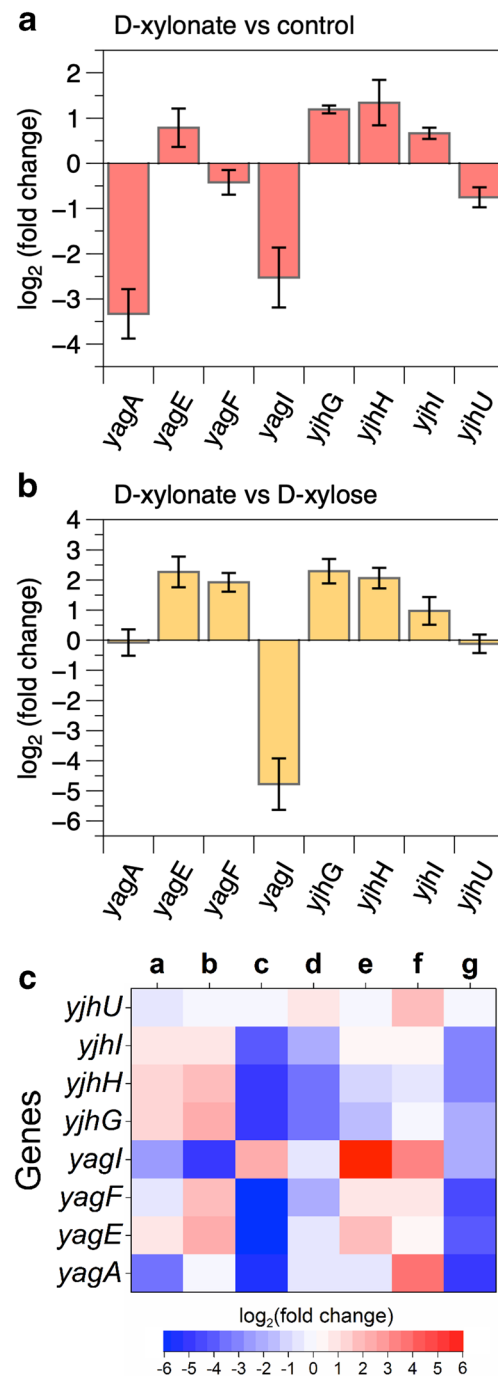

Fig. 2 Comparative gene expressions of *yag* and *yjh* genes in *E. coli* MG1655. $\log_2$(fold change) when cells are supplemented with 20 mM D-xylonate compared to cells grown on **a** MM9 medium only (control conditions) or **b** MM9 medium with 20 mM D-xylose. **c** Heat map for $\log_2$ (fold changes) for **a** D-xylonate-treated cells vs control; **b** D-xylonate-treated cells vs D-xylose-treated cells; **c** D-glucose-treated cells vs D-xylonate-treated cells; **d** (D-glucose + D-xylonate)-treated cells vs D-xylonate-treated cells; **e** (D-xylose + D-xylonate)-treated cells vs D-xylonate-treated cells; **f** (D-glucose + D-xylose + D-xylonate)-treated cells vs D-xylonate-treated cells; and **g** D-glucose-treated cells vs D-xylose-treated cells. Comparative C_T method was used to calculate the fold change values

showed that the P_{yagE} has high basal activity in the absence of D-xylonate (Fig. 3a) with RFU/OD$_{600}$ values slowly increased 4 h after D-xylonate induction. Meanwhile, no trends were observed in the P_{yagE} activity time profiles for the effect of D-xylose or D-glucose (Fig. 3b, c). In the case of P_{yjhI}, the fluorescence levels were very low prior to exposure with D-xylonate (Fig. 3a). Addition of D-xylonate resulted in a 25-fold increase in expression within 6 h, while treatment with D-xylose or D-glucose only showed background activity throughout the experiment (Fig. 3b, c). These results confirm that the promoters in question are activated/induced by the presence of D-xylonate, P_{yjhI} having better performance than P_{yagE}.

Overall, the results demonstrate that P_{yjhI} is involved in the positive regulation of $yjhI$, $yjhG$, and $yjhF$ gene expressions in response to D-xylonate. Although P_{yagE} initially exhibited a good response to D-xylonate during the expression analysis experiments (Fig. 2), it fared poorly in regulating the mCherry reporter protein compared to P_{yjhI} (Fig. 3). Hence, P_{yjhI} was further characterized and used in developing a synthetic genetic circuit. Identification of the cognate TF for P_{yjhI} was not pursued further in this study.

Characterization of the P_{yjhI} structure

In order to determine the essential DNA parts for transcription initiation, the 302-bp DNA sequence of P_{yjhI} was analyzed in silico using BPROM and NNPP (Reese 2001; Umarov and Solovyev 2017). Both programs predict the essential parts of the promoter sequence and transcription factor binding sites. BPROM analysis with a set score cutoff of > 0.90 predicted two potential promoter consensus regions, P_a and P_b (Fig. 4a, details shown in SI Fig. S3A). Meanwhile, NNPP analysis predicted two sites for Crp protein binding located within P_b (Fig. 4a, details shown in SI Fig. S3B). This supports the initial finding that P_{yjhI} activity may be subject to CCR. DNA curvature and % GC content analysis were also performed using the bend.it® online tool (Vlahoviček et al. 2003). The high curvature values and low GC content at the

P_b region (Fig. 4a) indicate increased probability for this DNA region to contain the sequences essential for P_{yjhI} promoter activity.

Deletion mapping experiment for P_{yjhI} was then performed to distinguish which of the two predicted sites (P_a or P_b) are essential for the promoter activity. Around 50-bp of DNA were removed sequentially from the 302-bp sequence of P_{yjhI} and the resulting 6 truncated fragments were individually cloned upstream of mCherry. As expected, the cells with the full sequence of P_{yjhI} showed increased red fluorescence at 24 h after induction with D-xylonate (Fig. 4b). The fluorescence observed in cells carrying truncated fragments up to Δ150 showed slightly lower values but were still around 10-fold higher than the negative control. Although the Δ150-deletion fragment effectively removed 80% of the P_a sequence, expression of mCherry remained unaffected. On the other hand, the Δ200-deletion fragment resulted in a drastic decline in fluorescence levels (Fig. 4b). This truncated fragment removed 48% of P_b sequence. Hence, the P_b region contains the potential RNA polymerase binding site while P_a may play a non-essential supporting role in P_{yjhI} activity.

To test the dynamic range of P_{yjhI} with D-xylonate, a dose-response experiment was performed (Fig. 4c). A 24-h time frame was selected since the fluorescent readout remained unsaturated even after 12 h in cells treated with > 40 mM D-xylonate (SI Fig. S4). Results show a 14-fold increase in fluorescent levels at the lower concentration range of D-xylonate (0 to 20 mM), which indicates excellent promoter sensitivity for P_{yjhI} (Fig. 4c). Higher D-xylonate concentrations only resulted in an incremental increase in the fluorescent readout. This may be attributed to the toxicity of D-xylonate at higher concentrations.

Thus far, the results show that P_{yjhI} has excellent performance in terms of background activity and response range to D-xylonate. The active promoter region was identified at position − 79 to − 124 from the start site (ATG) of the $yjhI$ gene and it contains the transcription start site, Crp binding sites, and the expected − 35 and − 10 sequence.
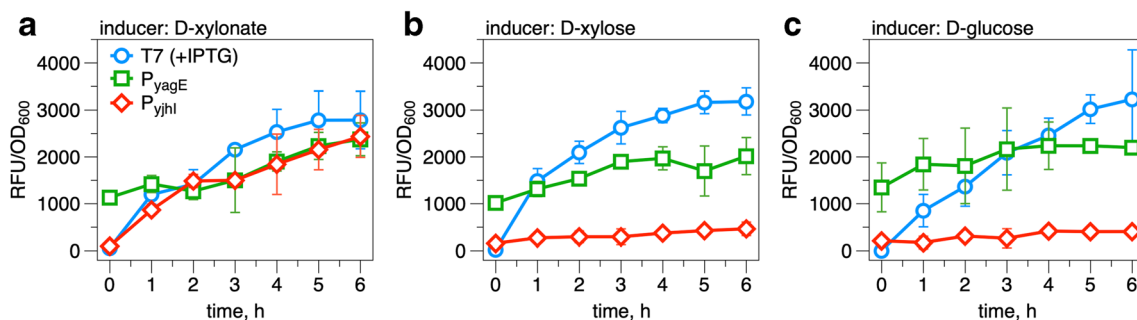

Fig. 3 Fluorescence of mCherry under the control of different promoters using D-xylonate (**a**), D-xylose (**b**), or D-glucose (**c**) as inducers. A final concentration of 20 mM inducer was added to the culture when OD$_{600}$ reached 0.4 A.U., at which the time was set as 0 h. MM9 media was used during cultivation. (RFU—mCherry fluorescence unit)
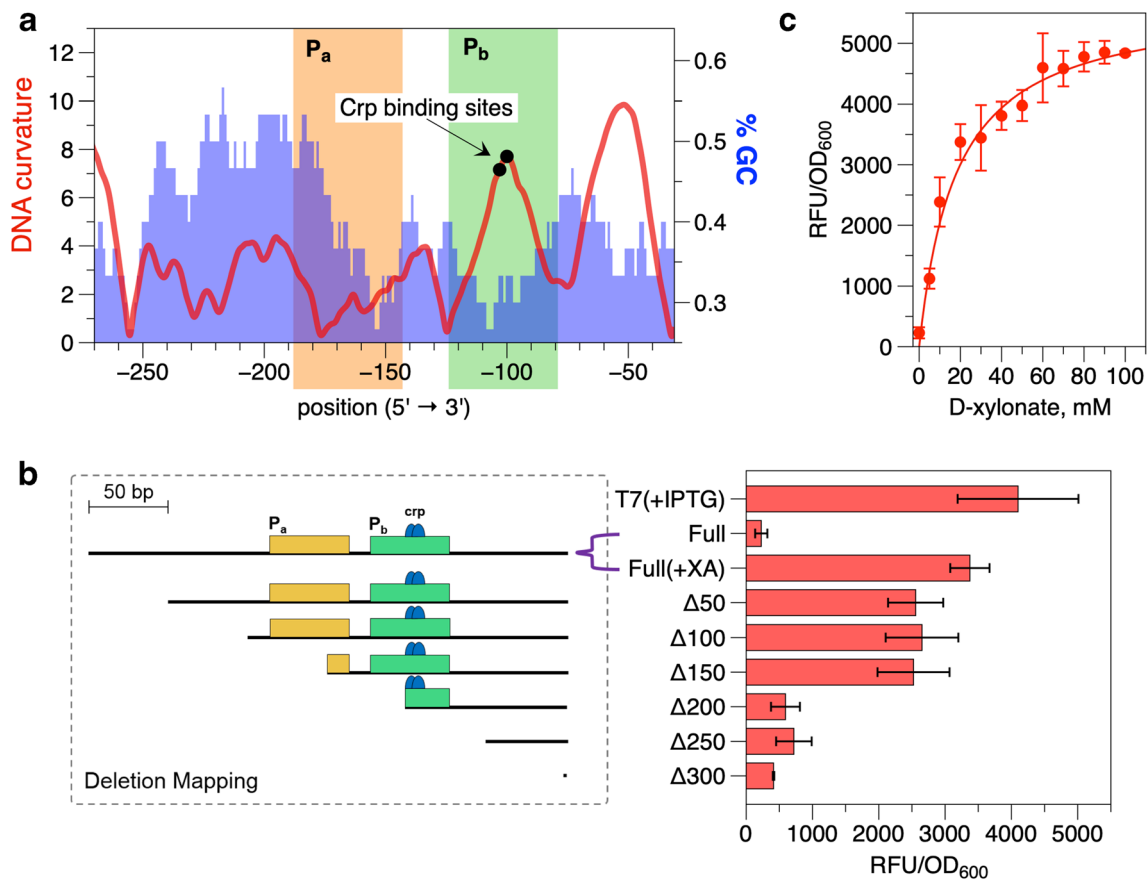
Fig. 4 Characterization of P_{yjhI}. **a** Predicted essential parts of the P_{yjhI} based on the results of BPROM, NNPP, and bend.it® analysis (SI Fig. S3). P_a and P_b are 5′-flanking DNA regions predicted to contain RNA polymerase binding sites. Position number is in reference to the start site (ATG) of the *yjhI* gene. **b** Deletion mapping experiment using mCherry expressed under different truncated fragments of P_{yjhI}. mCherry under the regulation of T7 promoter was used as positive control (T7+IPTG). *Full*

represents the full length of P_{yjhI} upstream of mCherry; (+XA) indicates induction with 20 mM D-xylonate. Strains expressing mCherry under the control of truncated fragments of P_{yjhI} (Δ symbol plus number of bases removed) are induced with 20 mM D-xylonate. **c** Dose response of P_{yjhI} towards D-xylonate. Samples were taken after 24-h cultivation. (RFU—mCherry fluorescence unit)

P_{yjhI}-driven genetic switch

As presented above, P_{yjhI} has the potential to detect and respond to D-xylonate and this was exploited to build a genetic switch (Fig. 5a). This P_{yjhI}-driven genetic switch is designed to activate the expression of downstream enzyme reactions that consume D-xylonate and simultaneously block D-xylonate accumulation through a feedback control. In this prototype genetic switch, mCherry was cloned downstream of $P_{T7-lacO}$ in a *lacI⁻* expression vector, which ensures the expression of mCherry in the absence of IPTG. The green fluorescent protein, *sf*GFP, and the repressor-coding gene, *lacI*, was then cloned separately downstream of P_{yjhI}. This allows the expression of both *sf*GFP and LacI only in the presence of D-xylonate; the *sf*GFP produces green fluorescence while the LacI repressor blocks the mCherry production (Fig. 5a). The complete genetic switch was integrated into a single vector, pR-XAS (SI Fig. S2).

To test the performance of the genetic switch, pR-XAS was transformed into *E. coli* W3110 (DE3). Preliminary tests using MM9 media without additional carbon source to support cellular growth revealed very low fluorescence, possibly due to carbon starvation which led to impaired growth (SI Fig. S5). Although, an exemption was observed in cells treated with D-xylonate. Under this treatment condition, better cell growth was observed and *sf*GFP expression was high since the host strain was capable of D-xylonate metabolism (Fig. 1a). Hence, cultivation was done in MM9 media with D-glucose to support cell growth. Two experimental conditions were set: (1) MM9 media with D-glucose only; and (2) MM9 media with D-glucose and induced with D-xylonate after 12 h. The D-glucose concentration used was 2.5 g L^{-1}, at which CCR effect was barely noticeable. High levels of mCherry and minimal *sf*GFP expressions were observed during the first 12 h of cultivation in both conditions (Fig. 5b). After 12 h of induction (24 h total cultivation time), a significant increase in GFU/OD$_{600}$ was observed in D-xylonate-treated cells while a 32% decrease in
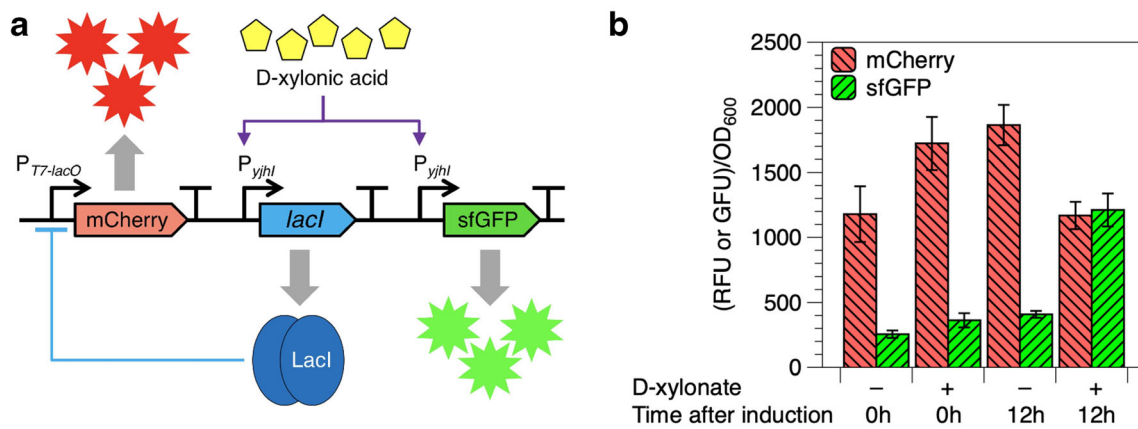
Fig. 5 **a** Designed dual-reporter synthetic genetic switch. mCherry is constitutively expressed in the absence of D-xylonate. Once D-xylonate is introduced, *sf*GFP expression is activated, as well as LacI which represses mCherry. **b** Fluorescence analysis of *E. coli* strains carrying the synthetic genetic switch. MM9 medium used containing 2.5 g L^{-1} D-

glucose to support growth. The cells were grown initially for 12 h to allow mCherry expression. A final concentration of 20 mM D-xylonate was used for induction. (RFU—mCherry fluorescence unit; GFU—*sf*GFP fluorescence unit)

RFU/OD$_{600}$ value was observed. Most of the red fluorescence still observed at 12 h after induction may be the consequence of the high protein maturation rate and photostability of mCherry compared to *sf*GFP (Kremers et al. 2007; Shu et al. 2006). On the other hand, the uninduced cells showed a significant increase in RFU/OD$_{600}$ levels while no significant change in GFU/OD$_{600}$ was observed (Fig. 5b). These results indicate that the designed P$_{yjhI}$-driven synthetic genetic switch worked properly and can be used for developing a D-xylonate biosensor or a D-xylonate-dependent genetic switch.

Synthetic D-xylonate switch for 1,2,4-butanetriol production

Synthetic genetic circuits were then built based on the prototype P$_{yjhI}$-driven synthetic genetic switch (Fig. 6). It should be able to impart dynamic control over the accumulation of D-xylonate in engineered microorganisms while improving the production of a target compound employing the Dahms pathway. In this work, BTO production was chosen to demonstrate the capabilities of the designed genetic switch since D-xylonate accumulation in this pathway is more prominent compared to systems producing ethylene glycol or glycolic acid from D-xylose (Cao et al. 2015; Sun et al. 2016; Valdehuesa et al. 2014; Wang et al. 2018).

The pathway for BTO production from D-xylose requires the expression of *xdh*, *mdlC*, and *yqhD* in an *E. coli* strain devoid of xylose isomerase (EC 5.3.1.5) and 2-keto-3-deoxy-D-xylonate dehydratase (EC 4.2.1.141) activities (Δ*xylAB* and Δ*yjhH*Δ*yagE*, respectively) (Valdehuesa et al. 2015; Valdehuesa et al. 2014). The *yjhH* and *yagE* gene knockouts were done such that the *yjhIHG* and *yagEF* mRNA transcripts contain the truncated version of the target

genes but still carries the rest of the functional genes (Valdehuesa et al. 2014). From the prototype P$_{yjhI}$-driven genetic switch, *xdh* was placed instead of mCherry while *mdlC* and *yqhD* for *sf*GFP (Fig. 6). This ensures adequate D-xylose uptake and its conversion to D-xylonate, while D-xylonate accumulation triggers the expression of the repressor LacI (reduces Xdh expression) and the downstream enzymes (for BTO production). A second strain was also constructed that lacks the feedback control mechanism mediated by D-xylonate-induced LacI repressor (partial system, Fig. 6). The complete genetic switch was introduced in *E. coli* W3110 (DE3) Δ*xylAB*Δ*yjhH*Δ*yagE* resulting in strain WBTXS while the partial genetic switch was designated as WBTC. For comparison purposes, a third strain designated as WBT+ was constructed which expressed all four genes for BTO production under the control of a strong constitutive promoter (Fig. 6).

BTO is a dead-end metabolite when produced from D-xylose through the Dahms pathway. Furthermore, the host strain carries deletion mutations in the *xylAB*, *yjhH*, and *yagE* genes. This means that BTO and the intermediate compounds in the pathway cannot be utilized by the cell for building cellular components. Hence, cell growth must be supported by using rich media or adding an extra carbon source in MM9 media during cultivation. In this part of the study, LB media was selected for BTO production to support cell growth and to circumvent any catabolite repression effect arising from using any sugar substrate.

Results show that the WBT+ strain produced 0.70 g L^{-1} BTO and accumulated 8.10 g L^{-1} D-xylonate (Fig. 7a) which is similar to the phenotype observed in the BTO-producing strain EWBT304 from a previous study (Valdehuesa et al. 2014). Unlike WBT+, the strain EWBT304 did not overexpress YjhG and YqhD, while Xdh and MdlC were
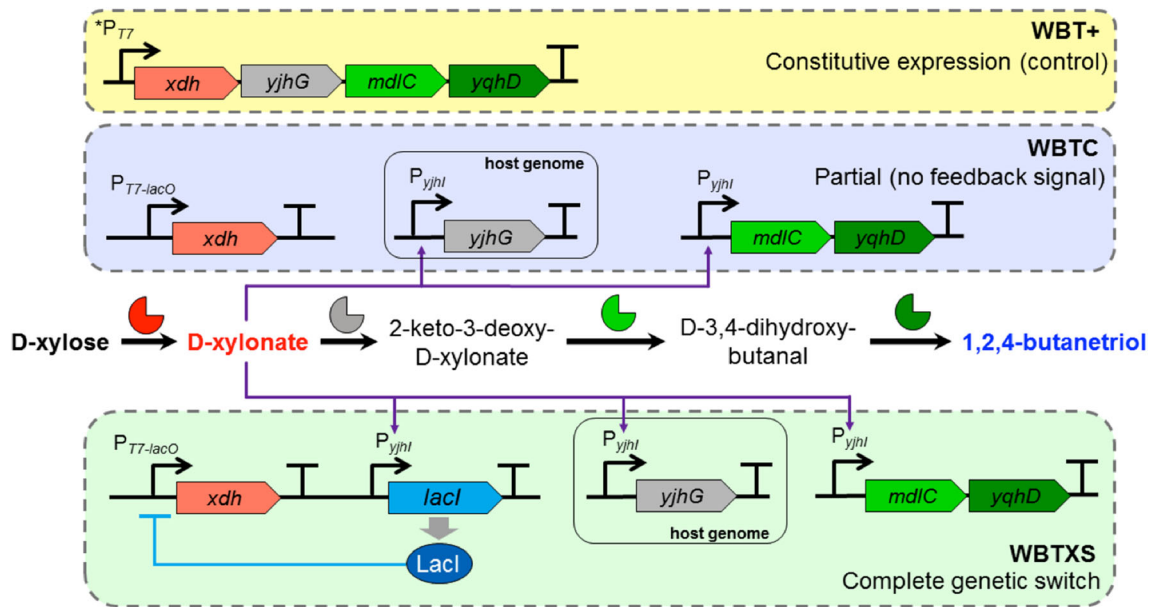
Fig. 6 Schematic diagrams for genetic constructs used in the production of BTO from D-xylose through the xylose oxidative pathway. The asterisk (*) indicates that the operon is expressed under the T7 promoter without the lac operator in a *lacI*-negative strain
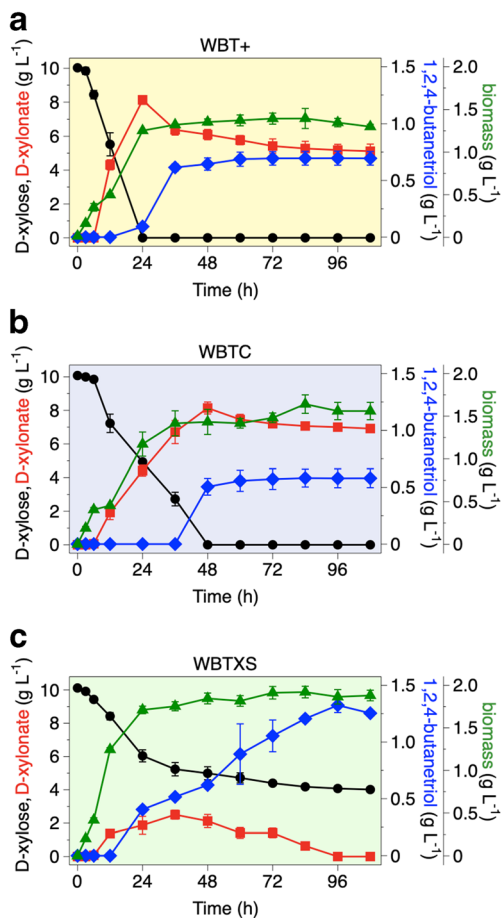

Fig. 7 Metabolite concentrations and growth profiles of BTO producing strains WBT+ (**a**), WBTC (**b**), and WBTXS (**c**). Shake-flask fermentations were performed with 10 g L^{-1} xylose and incubated at 37 °C for 108 h with 250-rpm agitation

constitutively expressed (Valdehuesa et al. 2014). From this information, it can be deduced that the issue on D-xylonate accumulation and low BTO production cannot be solved by simple overexpression of one or more genes, either constitutively or otherwise. For the WBTC strain, 0.58 g L^{-1} BTO was produced after 108 h of cultivation (Fig. 7b). D-Xylonate accumulated up to 8.1 g L^{-1} at 48 h which is similar to WBT+. The elevated D-xylonate concentration may have had influenced the lower biomass concentration compared to WBTXS (Fig. 7c). Growth tests for WBTC confirmed that biomass accumulation is 13–17% lower for conditions where extracellular concentrations of D-xylonate reach 4 g L^{-1} or higher (SI Fig. S6). This behavior is also observed in previous works (Cabulong et al. 2018b; Valdehuesa et al. 2014). Finally, the WBTXS strain fared better in terms of cell growth and BTO production (Fig. 7c). The highest concentration of D-xylonate accumulation was 2.5 g L^{-1} at 36 h and was gradually consumed by the end of the cultivation period. D-Xylose consumption slowed down during the stationary growth phase, having a final residual concentration of 4.0 g L^{-1} after 96 h. This is likely due to carbon starvation since the cells cannot catabolize the intermediate compounds of the BTO pathway. Furthermore, the intracellular NAD co-factor levels necessary for D-xylose conversion to D-xylonate may have also been depleted, thus preventing the cells to continue producing BTO (Cabulong et al. 2018b; Valdehuesa et al. 2014). The BTO production in WBTXS was 1.32 g L^{-1} at 96 h, a 2.2-fold increase compared to WBTC. This is equivalent to a yield of 0.31 mol mol^{-1} or 0.22 g g^{-1} (BTO/D-xylose consumed), which is 31% of the theoretical yield.

Discussion

The capability of *E. coli* K-12 strains and its derivatives to catabolize D-xylonate has been demonstrated in previous works (Liu et al. 2013; Liu et al. 2012; Valdehuesa et al. 2018). It involves the breakdown of D-xylonate to pyruvate through a succession of dehydration and aldol cleavage reactions (Fig. 1a). Interestingly, these two sequential reactions are reminiscent of the Dahms pathway (Dahms 1974). The enzymes for these reactions are encoded by the CP4-6 prophage-associated genes found in the *yag* and *yjh* gene clusters in the *E. coli* genome (Fig. 1b).

In order to complete Dahms pathway in *E. coli*, simple overexpression of the xylose dehydrogenase (*xdh*, EC 1.1.1.179) from *Caulobacter crescentus* (which oxidizes D-xylose to D-xylonate) is introduced on top of this inherent D-xylonate metabolic pathway (Liu et al. 2013). This has been instrumental in the conversion of D-xylose to ethylene glycol, glycolic acid, 1,4-butanediol, and polyhydroxyalkanoates (Cabulong et al. 2018a; Choi et al. 2016; Liu et al. 2013; Liu and Lu 2015). Earlier works on the optimization of this pathway also featured artificially induced expression of the dehydratases (EC 4.2.1.82), YagF or YjhG, and keto-pentonate aldolases (EC 4.1.2.18), YagE or YjhH, from the *yag* and *yjh* gene clusters in the *E. coli* genome (Fig. 1) (Valdehuesa et al. 2018). Although the actual physiological roles of these enzymes are currently unknown, recent reports have confirmed their activities in catalyzing certain reactions in the D-xylonate metabolic pathway (Jiang et al. 2015; Shimada et al. 2017). On the other hand, information concerning the native expression regulation of these enzymes is limited. It has been assumed that the presence of D-xylonate (from external addition or as a Dahms pathway intermediate metabolite) activates the expression of these enzymes, which then allows *E. coli* to grow on this sugar acid.

D-Xylonate-responsive promoters

In this work, the gene expression regulation of the aforementioned D-xylonate metabolic pathway in *E. coli* was explored further. The results of differential expression analysis and quantitative PCR experiments provided the first direct experimental evidence that the genes of the *yag* and *yjh* gene clusters are induced by D-xylonate (Fig. 2). Additionally, the promoter region upstream of the *yjhI* gene (P_{yjhI}) showed a better response to D-xylonate compared to P_{yagE} (located upstream of *yagE* gene) and was therefore selected for promoter characterization studies. Interestingly, these regions were previously identified to contain "constitutive promoters" through in vitro genomic SELEX screening (Shimada et al. 2014). Such in vitro study presented evidence for RNA polymerase binding onto P_{yjhI} and P_{yagE} in conditions lacking any interference from their cognate transcription factors (TF). This

does not directly contradict the results demonstrated in this work due to the difference in environmental conditions at which the experiments were conducted (in vitro vs in vivo). It is highly likely that these promoters interacted with their cognate TF in vivo. For example, the single-target TF called XynR (encoded by the *yagI* gene in the *yag* gene cluster) was reported to regulate the expression of the *yagEF* operon through its interaction with P_{yagE} (Shimada et al. 2017). Hence, gene knockout of *yagI* would render a "constitutive" behavior for P_{yagE} promoter in vivo.

Synthetic genetic switch and its application to BTO production

A persistent drawback in employing the Dahms pathway in *E. coli* is D-xylonate accumulation (Valdehuesa et al. 2018). Attempts to overcome this problem has been reported previously which demonstrated the use of traditional metabolic engineering strategies (Cabulong et al. 2018a; Cabulong et al. 2017). An alternative to these techniques is to utilize biosynthetic tools that confer dynamic regulation and control over D-xylonate accumulation. This requires genetic parts wherein the on-off response is triggered by a target signal molecule (Chen et al. 2012; Venayak et al. 2015). Since P_{yjhI} showed a good response to the presence of D-xylonate, it was then utilized to build a synthetic genetic switch which is aimed at providing dynamic control over D-xylonate accumulation (Fig. 6).

Apart from successfully limiting D-xylonate accumulation, the use of the genetic switch also contributed to the enhancement of BTO production (Fig. 7). Earlier reports on direct microbial fermentation of D-xylose to BTO in *E. coli* were able to achieve only 0.13 to 0.28 mol mol^{-1} yield from D-xylose (Cao et al. 2015; Sun et al. 2016; Valdehuesa et al. 2014; Wang et al. 2018). These works made use of traditional metabolic engineering techniques which included knockout of competing reactions, selection and overexpression of optimal enzymes, promoter strength modulation, and pathway optimization. Hence, the P_{yjhI}-driven switch has proven effective in delivering dynamic control over D-xylonate accumulation while greatly improving BTO yield from direct microbial fermentation of D-xylose. Other studies that implemented BTO production through cell-free systems or whole-cell biocatalysts reported high titer and yields (Gao et al. 2019; Hu et al. 2018). However, cell-free conversions require multiple expression strains for individual enzymes, which require purification through expensive affinity chromatography, and the addition of costly co-factors such as NAD(H). Meanwhile, whole-cell biocatalyst systems need several preliminary operations (high-density cell growth, harvesting, and then inoculation) before the actual biocatalytic conversion. The direct microbial fermentation strategy with an integrated dynamic genetic switch shown in this work, therefore, merits

recognition due to its process simplicity and promising cost-effectiveness.

Overall, this study presented a simple and dynamic genetic switch controller for D-xylonate in recombinant *E. coli*. This was achieved through a combination of molecular techniques and synthetic biology tools to identify the necessary and novel genetic parts, which were the basis for the constructed genetic circuit. Quantitative and relative expression analysis experiments revealed two D-xylonate-inducible operons, *yagEF* and *yjhIHG*, from *E. coli* which are flanked at the 5′-end with promoters P_{yagE} and P_{yjhI}, respectively. Based on its low background activity and wide range of response to D-xylonate, P_{yjhI} was selected for assembling a synthetic genetic switch. This contains a feedback control for the autoregulation of D-xylonate accumulation and expression activation of genes for BTO production. The P_{yjhI}-driven genetic switch effectively reduced D-xylonate accumulation which resulted in 31% BTO molar yield. This is the highest yield achieved thus far for direct microbial fermentation of D-xylose through the Dahms pathway. Further modifications and optimization of the P_{yjhI}-driven genetic switch may be done so it can be used in the microbial production of other compounds from D-xylose.

Compliance with ethical standards

Conflict of interest The authors declare that they have no conflict of interest.

Compliance with ethical standards This article does not contain any studies with human participants performed by any of the authors.

References

Beisel CL, Afroz T (2016) Rethinking the hierarchy of sugar utilization in bacteria. J Bacteriol 198:374–376. https://doi.org/10.1128/JB.00890-15

Brouns SJJ, Walther J, Snijders APL, van de Werken HJG, Willemen HLDM, Worm P, de Vos MGJ, Andersson A, Lundgren M, Mazon HFM, van den Heuvel RHH, Nilsson P, Salmon L, de Vos WM, Wright PC, Bernander R, van der Oost J (2006) Identification of the missing links in prokaryotic pentose oxidation pathways: evidence for enzyme recruitment. J Biol Chem 281:27378–27388. https://doi.org/10.1074/jbc.M605549200

Cabulong RB, Valdehuesa KNG, Ramos KRM, Nisola GM, Lee W-K, Lee CR, Chung W-J (2017) Enhanced yield of ethylene glycol production from D-xylose by pathway optimization in *Escherichia coli*. Enzym Microb Technol 97:11–20. https://doi.org/10.1016/j.enzmictec.2016.10.020

Cabulong RB, Lee W-K, Bañares AB, Ramos KRM, Nisola GM, Valdehuesa KNG, Chung W-J (2018a) Engineering *Escherichia coli* for glycolic acid production from D-xylose through the Dahms pathway and glyoxylate bypass. Appl Microbiol Biotechnol 102:2179–2189. https://doi.org/10.1007/s00253-018-8744-8

Cabulong RB, Valdehuesa KNG, Bañares AB, Ramos KRM, Nisola GM, Lee W-K, Chung W-J (2018b) Improved cell growth and biosynthesis of glycolic acid by overexpression of membrane-bound pyridine nucleotide transhydrogenase. J Ind Microbiol Biotechnol 46:159–169. https://doi.org/10.1007/s10295-018-2117-2

Cao Y, Niu W, Guo J, Xian M, Liu H (2015) Biotechnological production of 1,2,4-butanetriol: an efficient process to synthesize energetic material precursor from renewable biomass. Sci Rep 5: 18149. https://doi.org/10.1038/srep18149

Chen YY, Galloway KE, Smolke CD (2012) Synthetic biology: advancing biological frontiers by building synthetic systems. Genome Biol 13:240. https://doi.org/10.1186/gb-2012-13-2-240

Choi SY, Park SJ, Kim WJ, Yang JE, Lee H, Shin J, Lee SY (2016) One-step fermentative production of poly(lactate-co-glycolate) from carbohydrates in *Escherichia coli*. Nat Biotechnol 34: 435–440. https://doi.org/10.1038/nbt.3485

Chung CT, Niemela SL, Miller RH (1989) One-step preparation of competent *Escherichia coli*: transformation and storage of bacterial cells in the same solution. Proc Natl Acad Sci U S A 86:2172–2175

Dahms AS (1974) 3-Deoxy-D-pentulosonic acid aldolase and its role in a new pathway of D-xylose degradation. Biochem Biophys Res Comm 60:1433–1439. https://doi.org/10.1016/0006-291X(74)90358-1

Gao Q, Wang X, Hu S, Xu N, Jiang M, Ma C, Yang J, Xu S, Chen K, Ouyang P (2019) High-yield production of D-1,2,4-butanetriol from lignocellulose-derived xylose by using a synthetic enzyme cascade in a cell-free system. J Biotechnol 292:76–83. https://doi.org/10.1016/j.jbiotec.2019.01.004

Gibson DG, Young L, Chuang R-Y, Venter JC, Hutchison CA, Smith HO (2009) Enzymatic assembly of DNA molecules up to several hundred kilobases. Nat Meth 6:343–345. https://doi.org/10.1038/nmeth.1318

Görke B, Stülke J (2008) Carbon catabolite repression in bacteria: many ways to make the most out of nutrients. Nat Rev Microbiol 6:613–624. https://doi.org/10.1038/nrmicro1932

Green MR, Sambrook J (2012) Molecular cloning: a laboratory manual, 4th edn. Cold Spring Harbor Laboratory Press, New York

Hu S, Gao Q, Wang X, Yang J, Xu N, Chen K, Xu S, Ouyang P (2018) Efficient production of D-1,2,4-butanetriol from D-xylose by engineered *Escherichia coli* whole-cell biocatalysts. Front Chem Sci Eng 12:772–779. https://doi.org/10.1007/s11705-018-1731-x

Jiang Y, Liu W, Cheng T, Cao Y, Zhang R, Xian M (2015) Characterization of D-xylonate dehydratase YjhG from *Escherichia coli*. Bioengineered 6:227–232. https://doi.org/10.1080/21655979.2015.1040208

Kremers G-J, Goedhart J, van den Heuvel DJ, Gerritsen HC, Gadella TWJ (2007) Improved green and blue fluorescent proteins for expression in bacteria and mammalian cells. Biochemistry 46:3775–3783. https://doi.org/10.1021/bi0622874

Liu H, Lu T (2015) Autonomous production of 1,4-butanediol via a *de novo* biosynthesis pathway in engineered *Escherichia coli*. Metab Eng 29:135–141. https://doi.org/10.1016/j.ymben.2015.03.009

Liu H, Valdehuesa KNG, Nisola GM, Ramos KRM, Chung W-J (2012) High yield production of D-xylonic acid from D-xylose using engineered *Escherichia coli*. Bioresour Technol 115:244–248. https://doi.org/10.1016/j.biortech.2011.08.065

Liu H, Ramos KRM, Valdehuesa KNG, Nisola GM, Lee W-K, Chung W-J (2013) Biosynthesis of ethylene glycol in *Escherichia coli*. Appl Microbiol Biotechnol 97:3409–3417. https://doi.org/10.1007/s00253-012-4618-7

Pédelacq J-D, Cabantous S, Tran T, Terwilliger TC, Waldo GS (2006) Engineering and characterization of a superfolder green fluorescent protein. Nat Biotechnol 24:79–88. https://doi.org/10.1038/nbt1172

Radek A, Krumbach K, Gätgens J, Wendisch VF, Wiechert W, Bott M, Noack S, Marienhagen J (2014) Engineering of *Corynebacterium glutamicum* for minimized carbon loss during utilization of D-xylose containing substrates. J Biotechnol 192:156–160. https://doi.org/10.1016/j.jbiotec.2014.09.026

Reese MG (2001) Application of a time-delay neural network to promoter annotation in the *Drosophila melanogaster* genome. Comput Chem 26:51–56. https://doi.org/10.1016/S0097-8485(01)00099-7

Salusjärvi L, Toivari M, Vehkomäki M-L, Koivistoinen O, Mojzita D, Niemelä K, Penttilä M, Ruohonen L (2017) Production of ethylene glycol or glycolic acid from D-xylose in *Saccharomyces cerevisiae*. Appl Microbiol Biotechnol 14:127–113. https://doi.org/10.1007/s00253-017-8547-3

Shimada T, Yamazaki Y, Tanaka K, Ishihama A (2014) The whole set of constitutive promoters recognized by RNA polymerase RpoD holoenzyme of *Escherichia coli*. PLoS One 9:e90447. https://doi.org/10.1371/journal.pone.0090447

Shimada T, Momiyama E, Yamanaka Y, Watanabe H, Yamamoto K, Ishihama A (2017) Regulatory role of XynR (YagI) in catabolism of xylonate in *Escherichia coli* K-12. FEMS Microbiol Lett 364:2926. https://doi.org/10.1093/femsle/fnx220

Shu X, Shaner NC, Yarbrough CA, Tsien RY, Remington SJ (2006) Novel chromophores and buried charges control color in mFruits. Biochemistry 45:9639–9647. https://doi.org/10.1021/bi060773l

Solovyev VV, Salamov A (2011) Automatic annotation of microbial genomes and metagenomic sequences. In: Li RW (ed) Metagenomics and its applications in agriculture, biomedicine and environmental studies. Nova Science Publishers, New York, pp 61–78

Stephens C, Christen B, Fuchs T, Sundaram V, Watanabe K, Jenal U (2007) Genetic analysis of a novel pathway for D-xylose metabolism in *Caulobacter crescentus*. J Bacteriol 189:2181–2185. https://doi.org/10.1128/JB.01438-06

Sun L, Yang F, Sun H, Zhu T, Li X, Li Y, Xu Z, Zhang Y (2016) Synthetic pathway optimization for improved 1,2,4-butanetriol production. J Ind Microbiol Biotechnol 43:67–78. https://doi.org/10.1007/s10295-015-1693-7

Umarov RK, Solovyev VV (2017) Recognition of prokaryotic and eukaryotic promoters using convolutional deep learning neural networks. PLoS One 12:e0171410. https://doi.org/10.1371/journal.pone.0171410

Valdehuesa KNG, Liu H, Ramos KRM, Park SJ, Nisola GM, Lee W-K, Chung W-J (2014) Direct bioconversion of D-xylose to 1,2,4-butanetriol in an engineered *Escherichia coli*. Process Biochem 49:25–32. https://doi.org/10.1016/j.procbio.2013.10.002

Valdehuesa KNG, Lee W-K, Ramos KRM, Cabulong RB, Choi J, Liu H, Nisola GM, Chung W-J (2015) Identification of aldehyde reductase catalyzing the terminal step for conversion of xylose to butanetriol in engineered *Escherichia coli*. Bioprocess Biosyst Eng 38:1761–1772. https://doi.org/10.1007/s00449-015-1417-4

Valdehuesa KNG, Ramos KRM, Nisola GM, Bañares AB, Cabulong RB, Lee W-K, Liu H, Chung W-J (2018) Everyone loves an underdog: metabolic engineering of the xylose oxidative pathway in recombinant microorganisms. Appl Microbiol Biotechnol 102:7703–7716. https://doi.org/10.1007/s00253-018-9186-z

Venayak N, Anesiadis N, Cluett WR, Mahadevan R (2015) Engineering metabolism through dynamic control. Curr Opin Biotechnol 34:142–152. https://doi.org/10.1016/j.copbio.2014.12.022

Vlahoviček K, Kaján L, Pangor S (2003) DNA analysis servers: plot.it, bend.it, model.it and IS. Nucl Acids Res 31:3686–3687. https://doi.org/10.1093/nar/gkg559

Wang X, Xu N, Hu S, Yang J, Gao Q, Xu S, Chen K, Ouyang P (2018) D-1,2,4-Butanetriol production from renewable biomass with optimization of synthetic pathway in engineered *Escherichia coli*. Bioresour Technol 250:406–412. https://doi.org/10.1016/j.biortech.2017.11.062

Weimberg R (1961) Pentose oxidation by *Pseudomonas fragi*. J Biol Chem 236:629–635

Xu P, Vansiri A, Bhan N, Koffas MAG (2012) ePathBrick: a synthetic biology platform for engineering metabolic pathways in *E. coli*. ACS Synth Biol 1:256–266. https://doi.org/10.1021/sb300016b

Zhang N, Wang J, Zhang Y, Gao H (2016) Metabolic pathway optimization for biosynthesis of 1,2,4-butanetriol from xylose by engineered *Escherichia coli*. Enzym Microb Technol 93-94:51–58. https://doi.org/10.1016/j.enzmictec.2016.07.007